Chemical, structural and physical characterisation of the synthesis of WC-TIC particles using a radio frequency plasma

Rearabetswe Dire[1*], *Hertzog* Bissett[2], *Kasturie* Premlall[3], *Milton* Makhofane[4]

[1*, 3] Department of Chemical Engineering, Tshwane University of Technology, South Africa
[2,4] The South African Nuclear Energy Corporation SOC Ltd. (Necsa), South Africa

Abstract. The formation of a tungsten titanium carbide alloy results in the enhancement of high temperature strength and the improvement of resistance to wear, oxidisation and corrosion. A WC-TiC alloy was produced by a novel radio frequency plasma process. The starting material varied in Ti content in the range 1-15%. The chemical and structural characteristics of the WC-TiC alloy were analysed with respect to the Ti to W ratio. The powder will be used to fabricate a dense part using a spark plasma sintering.

1 Introduction

New innovative alloys can improve material strength, wear and corrosion resistance for various industrial applications [1]. For example the addition of titanium carbide (TiC) in small amounts, ranging between 1 and 15%, into tungsten (W) metal produces W-TiC composite material enhancing the ability of the material to withstand high temperatures, improve resistance to wear, corrosion and oxidation [2]. The metal composite also dispenses with metallic binders such as Co, Ni, Fe, in cemented carbide cutting tools, wear resistance parts and mechanical seals [3]. Small amounts of TiC (< 10 wt.%) is usually added into WC based cutting tools to provide primary resistance to cratering.

The purpose of this study is to form a tungsten titanium carbide alloy by exposing elemental tungsten and titanium powders to methane gas in a Tekna 15 kW radio frequency (RF) plasma torch at high temperatures. This approach is novel.

2 Methodology

Thermodynamic evaluation of producing WC-TiC composite/alloy from a mixture of W, Ti and CH_4 was performed using its equilibrium model. This model predicts the equilibrium composition of the mixture as function of temperature [4].

Pure tungsten (material no: GF31027463-1EA) and titanium (material no: GF31074308-1EA) with a maximum particle diameter of 100 µm and 75 µm respectively was purchased (Merck Life Science (Pty) Ltd).

The Ti powder was mixed with the W powder in ratios ranging between 1-15% (Ti into W). The formation of the alloy occurred in a RF plasma with hydrogen (H_2) and argon (AR) as the sheath gas and methane (CH_4) as the carrier gas to form tungsten titanium carbide. All powders were treated at a power of 15kW with a feed rate of 6.04g/min. Powder products were collected from the cyclone (mixture of nano & micro particles) and the filter (nano

* Corresponding author: rearabetswedire@gmail.com

particles) after the experiment. More detail regarding the experimental set-up can be found in a previous paper [5].

Structural and chemical characterisation of the powders were determined through X-ray diffraction (XRD) using the ICDD (International Centre for Diffraction Data) database. Qualitative identification of the chemical phases is done using the Search/Match technique where the measured diffraction peaks (intensities and peak positions) are matched against the known patterns from ICDD PDF-4+ 2023 database entries using the Sieve+ software package.

The density analyses of the W-Ti powders were done by helium pycnometry.

The SEM analysis of the W-Ti powders was conducted using the Scanning Electron Microscopy (SEM) with Energy Dispersive X-ray Spectroscopy (EDS) at a voltage of 20kV. A magnification used was between 155x and 3000x was used to determine general morphology and detail the specific microstructural features.

The particle size distribution (PSD) of the W-Ti powders was determined using a laser diffraction technique via the Saturn DigiSizer II 5205 instrument. This method provides high-resolution measurement of particle sizes based on light scattering.

Figure 1 provides a visual representation of the experimental, analysis and characterisation route followed. The figure depicts the four powder mixtures, the RF plasma used to treat the powder in the presence of CH_4 and the powder collected from the cyclone (mixture of nana & micro particles) followed by the sequence of characterisation and analysis procedures.

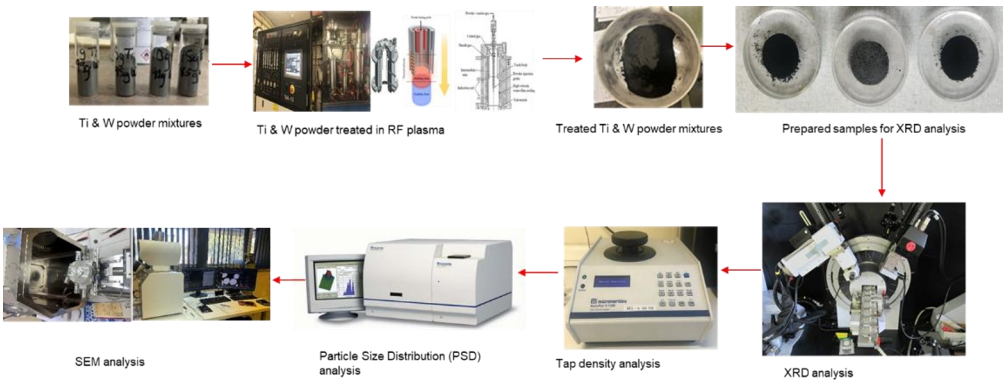

Fig. 1. Experimental procedure and XRD, tap density & SEM analysis and characterisation methodology.

3 Results

Figure 2 depicts the thermodynamic calculations results for the reaction of Ti and W in the presence of CH_4. The figure revealed that WC concentration increase from ambient temperature until a temperature of 500 °C. Possible reduction of WC to W and C by H_2 from decomposed CH_4 is responsible for the decreasing concentration of WC. TiC was found to be stable until a temperature of 2000 °C. Reduction of TiC to Ti is observed above 2000 °C.

The thermodynamic predictions HSC Chemistry at high temperatures are strongly supported by the experimental findings of Davidson et al. **[7]**. Their work demonstrated that:

- Tungsten reacts with methane gas at high temperatures (~1000–1500°C) through a surface-controlled reaction pathway.

- The initial phase formed during carburization is W_2C (tungsten semi-carbide), which later transforms into WC (tungsten carbide) as carbon activity increases.
- The reaction mechanism involves adsorption of methane on the tungsten surface, followed by decomposition and carbon diffusion into the metal lattice.

Zang et al. **[8]** found that in the reaction between titanium dioxide and methane, the effective TiC formation begins at temperatures above 1300°C, with complete conversion typically observed above 1500°C under optimal methane concentration. The methane gas decomposes thermally into hydrogen and active carbon species, which react with the oxygen in TiO_2 to form CO and leave behind titanium carbide (TiC). The findings of both Davidson et al and Zang et al. support the HSC results of the formation of Ti & WC occurs at elevated temperature of 1500°C and higher.

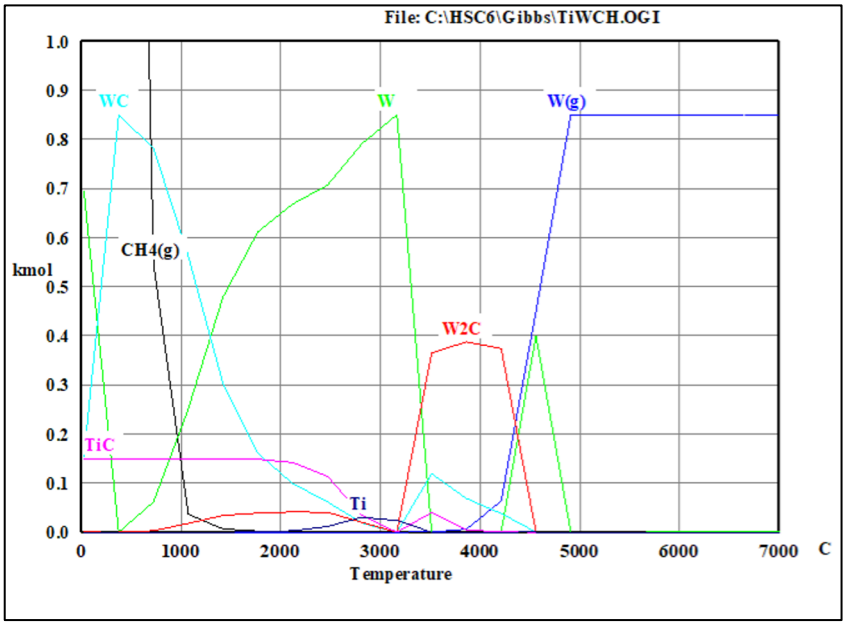

Fig. 2. HSC results of reaction of Ti & W with CH_4.

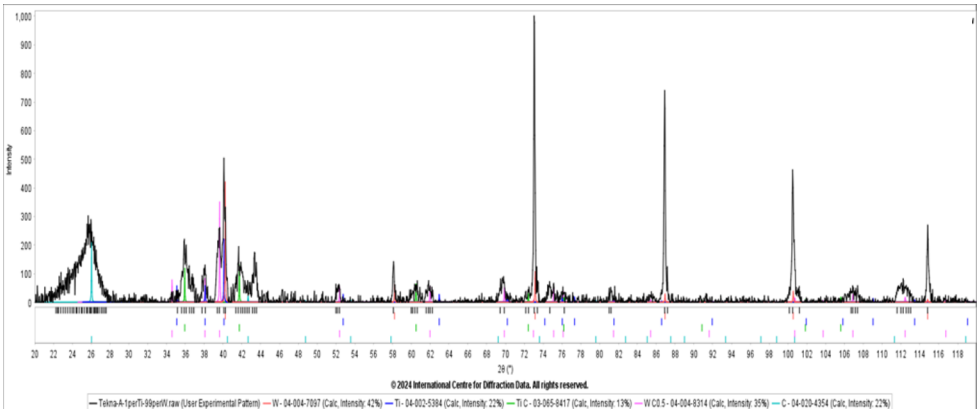

Fig. 3. Software processed diffraction pattern of Tekna sample of a mixture of 1% Ti and 99% W (black trace) overlaid with stick patterns of proposed phases, W (red sticks), Ti (blue trace), TiC (green trace), WC (magenta trace) and C (cyan trace). Inset pie chart indicates the proposed phases with corresponding phase concentration in wt%.

Figure 3 depicts diffraction patterns of the Tekna treated 1% Ti and 99% W mixture which are superimposed with stick patterns of identified phases of titanium, tungsten, titanium carbide, tungsten carbide and carbon. The Ti phases where are observed at the following phases and intensities: 41º with intensity of 390, 58º with intensity of 500, 86º & 101º with intensity of 400 and 113º with intensity of 100. All the phases were narrow. The narrow diffraction peaks of the tungsten powder suggest that there is high crystallinity, large crystallite size and that there are low macrostrain or defects.

The titanium peaks where identified with the following intensities: 35º with intensity of 70, 38º with intensity of 50, 40º with intensity of 248 and 63º with intensity of 25. The minimal identification of Ti peaks speaks to the 1% of Ti present in the mixture. The observed peaks were also narrow diffraction peaks which suggest that there is high crystallinity, large crystallite size and that there are low macrostrain or defects. The titanium carbide (TiC) peaks where identified at the following intensities: 38º with intensity of 148, 42º with intensity of 148, 60º with intensity of 50 and 72º with intensity of 50. The highest intensities were observed at 38º & 42º respectively. The low identification of the formation of TiC is due to the 1% of Ti present in the mixture.

The presence of tungsten dicarbide (WC_2) was identified at the following peaks and intensities: 35º with intensity of 99, 38º with intensity of 100, 40º with intensity of 350, 52º ,62º 50, 70º , 75º, 76ºwith intensity of 50, 85º with intensity of 25, 101º with intensity of 20, 105º with intensity of 20, 112º & 116º with intensity of 10. The presence of 13 peaks of WC_2 with low intensities suggest that there are multiple crystalline phases with complex compositions that exist within the powder mixture. The phases present in small quantities could be poorly crystalline or consist of nanocrystalline material.

There also carbon phases identified at the following peaks: 26º with an intensity of 200 and 43º with an intensity of 50. According to the XRD results of the treated powder in RF plasma in the presence of CH_4 , the powder was able to form titanium carbide and tungsten carbide respectively.

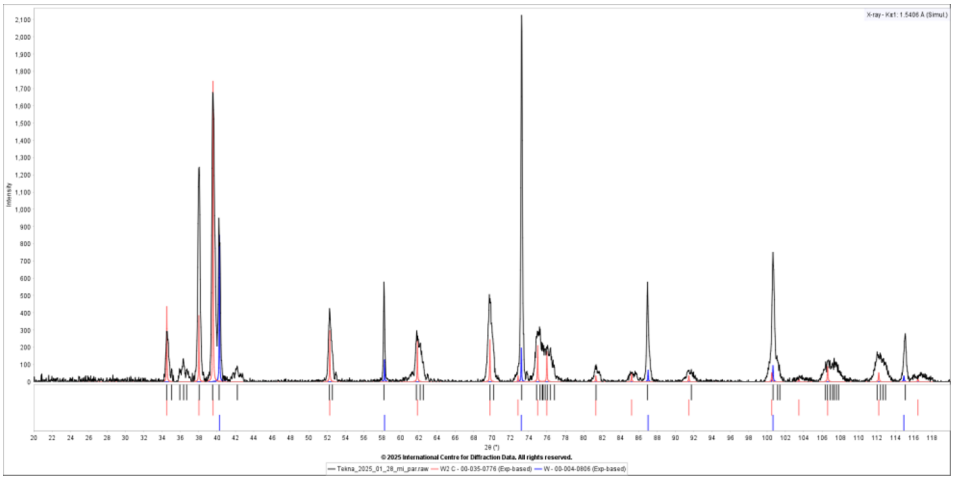

Fig. 4. Software processed diffraction pattern of the as-produced micron sized particle Tekna 5%Ti - 95%W composition (black trace) overlaid with stick patterns of the proposed phases of W & W_2C.

Figure 4 depicts the phases identified in the powder mixture of 5%Ti and 95% W mixture after treatment in the Tekna. From the figure the following tungsten (W) phases and intensities were identified: 40º with intensity of 800, 58º with intensity of 150, 73 with intensity of 200, 87º with intensity of 50, 101º with intensity of 100 and 115º with intensity of 50. Only 6 phases of W were identified which suggest that the W reacted to form new crystalline phases.

The ditungsten carbide phases were identified with the following intensities: 35º with intensity of 430, 38º with intensity of 400, 40º with intensity of 1750, 52º with intensity of 350, 62º with intensity of 250, 73º with intensity of 50, 75 & 76º with intensity of 200, 81º,85º, 91º with intensity of 50º, 107º with intensity of 100 and 112º with intensity of 50. At 40º both W and W_2C were identified with W_2C having a higher intensity with suggest that indeed new crystalline phases were formed which supports the low W phases observed.

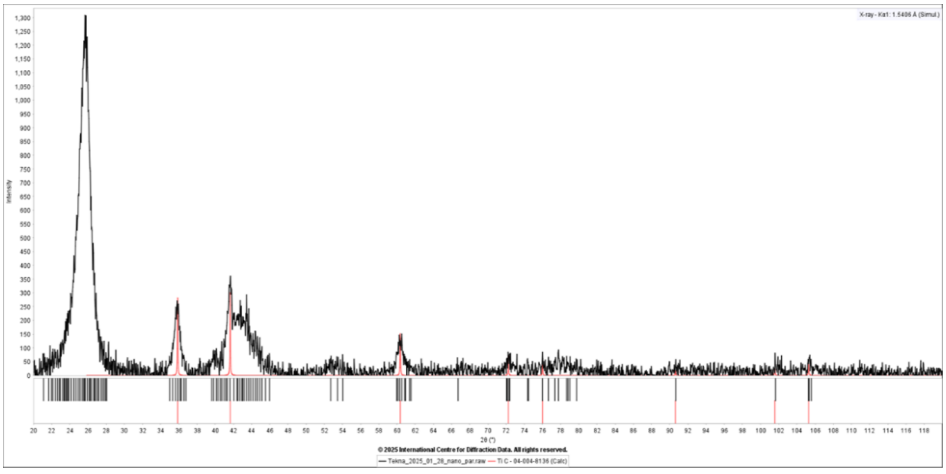

Fig. 5. Software processed diffraction pattern of the as-produced nano-sized particle Tekna 5%Ti - 95%W composition (black trace) overlaid with stick pattern of TiC (red sticks).

Figure 5 depicts the various TiC intensities, which were identified at the following peaks: 36º with intensity of 300, 42º with intensity of 350, 61º with intensity of 150, 72º with intensity of 50, 76º with intensity of 25, 91, 102º with intensity of 20 and 105º with intensity of 50. The results depict that indeed the powder mixture of 5%Ti and 95%W treated with CH_4 did react to form TiC, although the peaks and intensities are relatively low but the TiC crystalline new phase of TiC was formed.

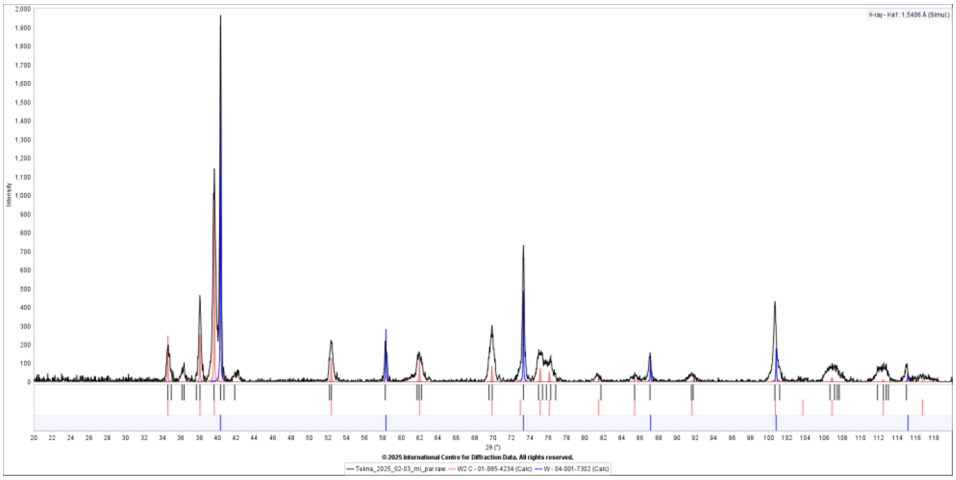

Fig. 6. Software-processed diffraction pattern of the as-produced micron sized particle Tekna 10%Ti - 90%W composition (black trace) overlaid with stick pattern of proposed phases W_2C (blue) and W (red).

From Figure 6 there are W_2C intensities identified at the following phases: 35º with intensity of 250, 38º with intensity of 250, 40º with intensity of 1000, 52º with intensity of 150, 62º with intensity of 100, 70º , 75 with intensity of 50 and 76 Software-processed diffraction pattern of the as-produced nano-sized particle Tekna 10%Ti -90%W composition (black trace) overlaid with stick patterns of the proposed phases.40, 82º, 85º, 92º, 100º, 105º, 113º, 117º with intensity of 30.

The W intensities were identified at the following phases: 40º with intensity of 2000, 58º with intensity of 300, 73º with intensity of 500, 87º with intensity of 100, 101º with intensity of 200 and 115º with intensity of 30. From the Figure 6 we can deduce that at 40º the W did form a new crystalline phase of W_2C.

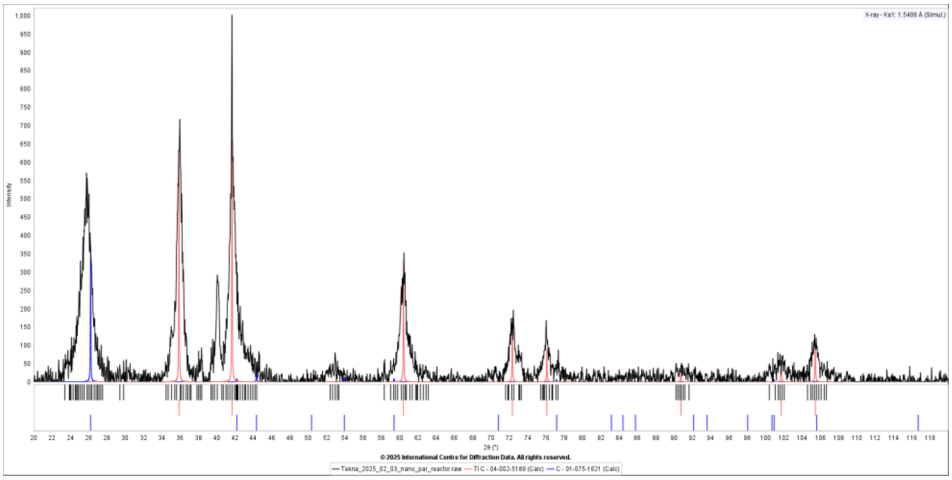

Fig. 7. Software-processed diffraction pattern of the as-produced nano-sized particle Tekna 10%Ti - 90%W composition (black trace) overlaid with stick patterns of the proposed phases TiC (red) W_2C (blue).

Figure 7 shows the identified peaks at the following phase of TiC: 36º with intensity of 650, 42º with intensity of 600, 72º with intensity of 150, 76º with intensity of 100, 91,102º with intensity of 50 and 105º with intensity of 100. The identification of the Ti phases indicate that Ti reacted with CH_4 to for TiC. Carbon phases were identified at the following intensities: 26º with intensity of 350, 5, 42, 45º with intensity of 20.

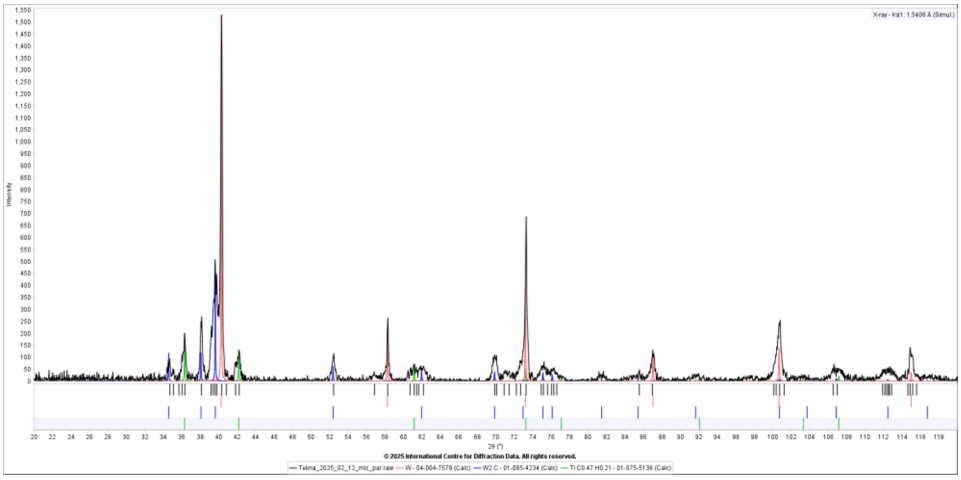

Fig. 8. Software-processed diffraction pattern of the as-produced micro sized particle Tekna 15% Ti – 85% W composition (black trace) overlaid with stick patterns of the proposed phases W (red), W_2C (blue).

From Figure 8 the following W phases were identified at the following intensities: 40º with intensity of 1000, 89º with intensity of 350, 73º with intensity of 400, 87º with intensity of 100, 101º with intensity of 150 and 113º with intensity of 40. With fewer phases identified it would support the assumption that the W reacted to form other crystalline phases with the mixture.

The following W_2C phases were identified at the following intensities: 35º with intensity of 150, 38º with intensity of 150, 40º with intensity of450, 53º with intensity of 50º, 62º with intensity of 50, 70º with intensity of 50, 75º 76º with intensity of 50. From figure 9 W and W_2C share a peak of 40º which indicated that W did react with CH_4 during treatment to form W_2C.

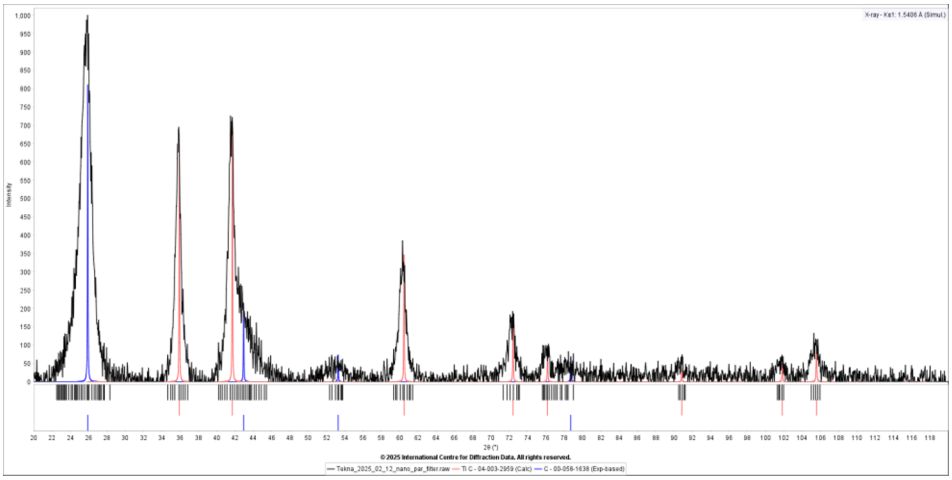

Fig. 9. Software-processed diffraction pattern of the as-produced nano sized particle Tekna 15%Ti - 85%W composition (black trace) overlaid with stick patterns of the proposed phases red (TiC) & blue (C).

The following TiC phases were identified at the following intensities: 36º with intensity of 650, 42º with intensity of 700, 61º with intensity of 400, 72º with intensity of 200, 76º with intensity of 100, 91º with intensity of 50 and 105º with intensity of 105. The presence of TiC phases in the powder mixture is an indication of the reaction of Ti with CH_4.

The XRD results revealed that WC, W_2C and TiC compositions were present in all Ti and W powder mixtures which indicated that the formation of TiC and WC compound during the RF treated in the presence of CH_4 did indeed yield the desired compositions.

Skeletal density analysis was performed on Ti–W powder mixtures containing varying weight percentages of titanium (1%, 5%, 10%, and 15%) using helium pycnometry. The results, are summarized in Table 1, reveal a non-linear trend in density as a function of titanium content.

Table. 1. Summary of skeletal density measurements for Ti–W composites after treatment in the Tekna plasma system.

Ti Content	W Content	Sample Mass (g)	Measured Volume (cm^3)	Average Density (g/cm^3)	Std. Deviation (g/cm^3)	Temperature (°C)
1% Ti	99% W	12.0855	0.6996	17.2743	0.0053	15.09
5% Ti	95% W	24.9680	1.4202	17.5808	0019	15.28
10% Ti	90% W	23.8859	1.4388	16.6008	0.0034	15.48
15% i	85% W	15.9734	1.1510	13.8776	0.0036	15.70

The skeletal density results of the powder mixtures exhibited a distinct decrease with increasing titanium percentage within the powder mixtures, which aligns with the intrinsic densities of both tungsten of 19.3 g/cm^3 and of titanium which is 4.5 g/cm^3. As the percentage of titanium increases, the overall mixture becomes less dense. Although, the 5% Ti–95% W sample exhibits a higher skeletal density of 17.5808 g/cm^3 in comparison to the 1% Ti–99% W powder sample of 17.2743 g/cm^3, which is counterintuitive. This may be due to:

- measurement variability, packing behaviour, or the presence of denser secondary phases at 5% Ti.
- SEM images and EDS data (figure 5) showed that the 5%Ti powder sample exhibited higher W concentrations in certain areas compared to the 1%Ti sample.

A density drop was observed at higher Ti concentration. An expected decrease in density is observed between 10% and 15% Ti, with a drop of 2.72 g/cm^3. This suggests a possible microstructural or phase transformation, such as:

- The possible formation of less dense titanium carbide (TiC) or complex Ti–C compounds (e.g., C_5Ti_8 or $TiC_{0.47}H_{0.21}$), as identified by XRD as stipulated above.
- Enhanced nanoparticle content, especially for samples collected from reactor filters.

The standard deviation of all samples was below 0.0054 g/cm^3, this indicates a high measurement reproducibility and minimal experimental variation. Temperatures were also consistent (15.1–15.7 °C), ensuring thermal stability during measurement.

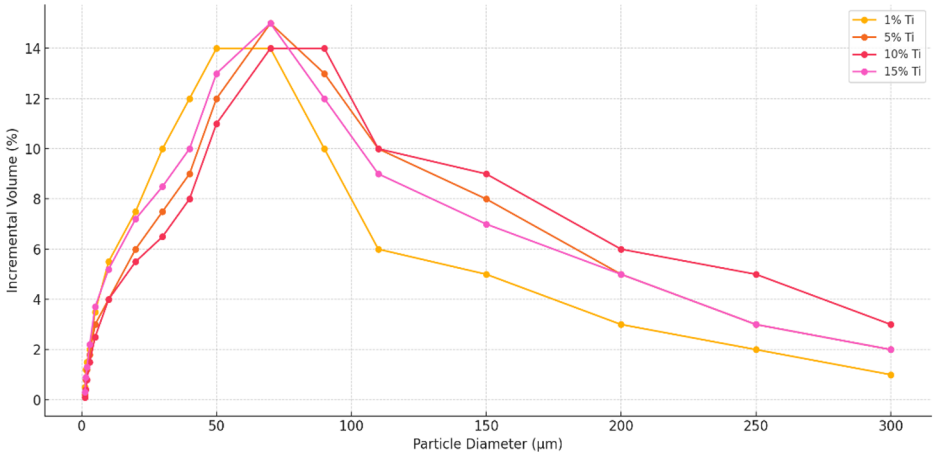

Fig. 10. Incremental volume vs. particle diameter graph for all four W-Ti powder samples.

In Figure 10 the particle size distribution of the various powder samples are displayed, while the D10, D50, D90 as well as the mean values are given in Table 2.

The 1% Ti and 99% W powder sample (yellow curve in Figure 10) depicts a peak position at 50 µm. The curve rises quickly and falls abruptly. The sample depicts a narrow, unimodal distribution observed on the median. This observation indicated a highly uniform particle size, which is desirable in many powder metallurgy processes [9]. The small D10 value (~1.5 µm) means there are very few fine particles, contributing to consistent flowability and predictable sintering behavior.

The 5% Ti and 95% W powder sample (orange curve in Figure 10) depicts a wider peak which spreads between ~30 µm to ~100 µm respectively. The curve shows a moderate skew; the curve skews slightly toward larger particle diameters. This indicates a broader distribution compared to the 1% Ti & 99% W powder sample. A higher D90 (~285 µm) is observed which supports that assumption that there is a presence of larger particles within the powder mixture. This particular particle distribution could enhance packing density in some applications, but might reduce uniformity and increase sintering heterogeneity.

The 10% Ti and 90% W powder sample (red curve in Figure 10) depicts a high mid-range peak. Observed between ~70–110 µm, the powder particle distribution is moderate which indicates a more uniform distribution in the mid to upper range. There are fewer fine particles (high D10 ~18 µm) observed and many mid-sized particles. While the distribution is broad, the gentle slope and moderate standard deviation suggest a well-distributed size profile that can improve powder flow and deposition consistency, especially in thermal spray or additive manufacturing [10].

The 15% Ti and 85% W powder sample (purple curve in Figure 10) depicted a broad particle distribution. The curve showed a dual slope pattern with a small rise for fine particles and a long tail of coarse particles. The curve showed patterns of hetero-disperse or multimodal distribution. The sample contained both very fine and very coarse particles (low D10 ~3.8 µm and high D90 ~282 µm). The observed particle size distribution offers high packing density, but may result in uneven compaction and non-uniform sintering, particularly problematic for precision applications.

Table. 2. Comparison of particle size analysis of all four samples of D10, D50, D90 and mean.

Ti %	D10 (µm)	D50 (µm)	D90 (µm)	Mean (µm)	Std Dev
1%	1.540	51.580	123.987	51.929	5.053
5%	6.584	67.333	285.228	90.904	11.049
10%	18.090	72.276	284.264	98.010	5.514
15%	3.797	89.553	282.506	105.503	11.111

Comparing the values given in Table 2 it can be seen that the sample containing 10% Ti had a much larger D10 value indicating that the finer fraction in this sample were larger particle compare to the other samples. The reason for this is due to the fact that during removal of fines from the reactor, not all fines were collected, resulting in an increase of the D10 values as seen in Table 2. Looking at the D50 value in Table 2 of the various samples, it can be seen that the amount of fines decreases with increased Ti amount. The reason for this is, because the Ti inhibits heat transfer thereby reducing fine particle formation. Also, with more Ti present, less fine particle formation results in agglomerate formatting as can be seen especially in the D90 values. With more Ti present, more large particles are found in the samples as seen from D50 and the Mean values in Table 2.

Each composition was analysed at multiple magnifications (1000× and 3000×), with EDS spectra captured for full areas, selected areas, and multiple localized spots.

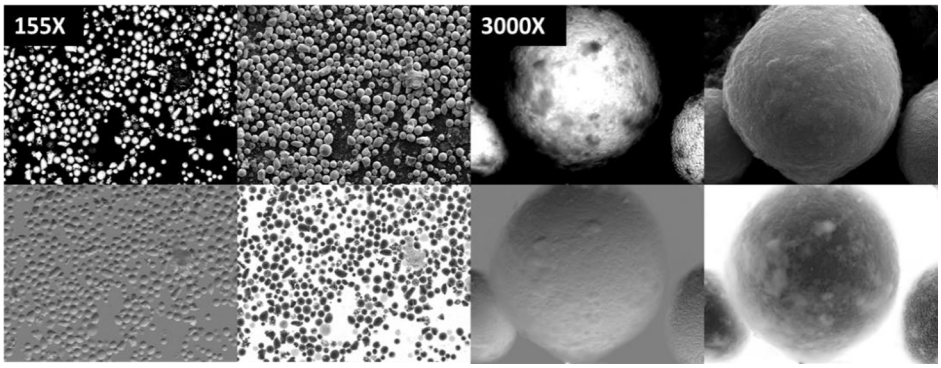

Fig. 11. SEM images of 1%Ti and 99% W at microscopic view at 155x and 3000x.

The 1%Ti and 99%W sample depicted a C-rich matrix. Most of the areas had over 75% C by weight, indicating a dominant carbonaceous matrix—likely graphite or WC. The presence of Ti was observed to be relatively low. The presence of Ti was detected typically between 0.5–1.3 wt%, which aligns with the original mixture composition.

There were W-rich zones observed. Several localized spots had up to 63% W, suggesting the presence of discrete tungsten particles. There were alloying particle traces observed one region at 1000× contained Cr, Fe, Ni — possibly from contamination or alloying. The sample exhibited a homogeneous matrix with embedded W-rich particles. The presence of Ti is minimal and uniformly dispersed.

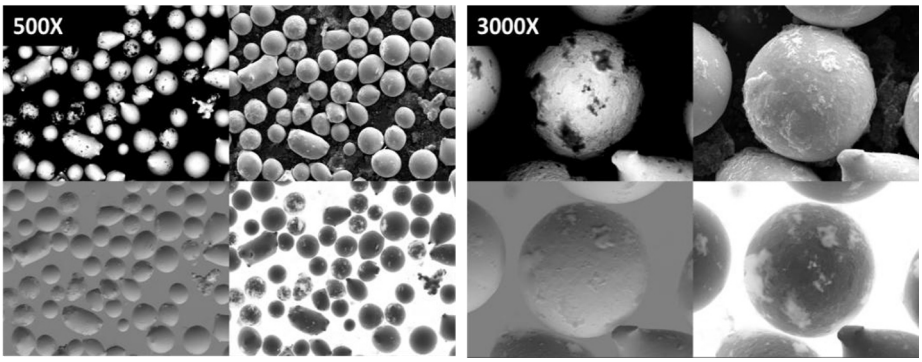

Fig. 12. SEM images of 5%Ti and 95% W at microscopic view at 500x and 3000x.

The SEM analysis of 5% Ti and 95% W depicted q wide of carbon content ranging from 18–81% wt, suggesting heterogeneous distribution. A large percentage of W is identified in certain EDS spots, especially in regions with lower carbon which indicating W agglomerates.

Ti detection is more consistent than in the 1%Ti 99% W sample (typically 1–4% wt, up to 18.9% in one location).

The SEM analysis depicts a greater heterogeneity, likely due to the increased Ti content observed altering the interaction between W and C phases. The distribution pattern suggests some localized Ti enrichment.

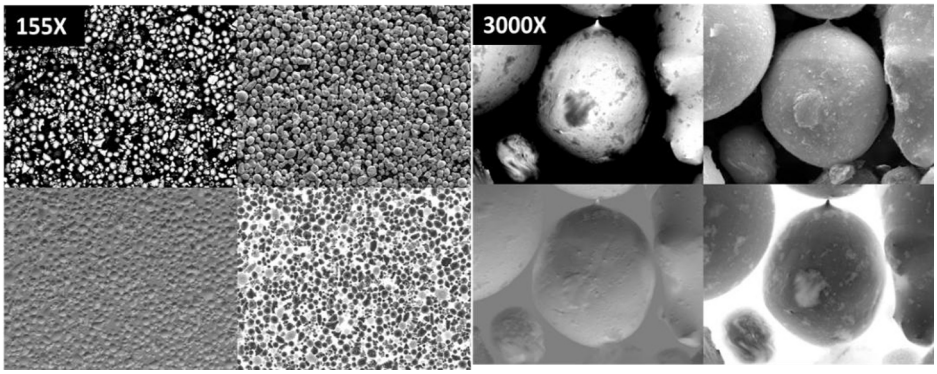

Fig. 13. SEM images of 10% Ti and 90% W at microscopic view of 155x and 3000x.

The SEM analysis of 10%Ti and 90% W At 3000×, exhibits that the C and W phases are co-dominant with an average of ~48% each in some regions. Local EDS spots indicated up to 84.5% W or as low as 19% W depending on the zone area. The presence of Ti varies widely ranging between 1–36 wt% in spots, indicating strong compositional inhomogeneity.

The 10% Ti and 90% W sample exhibited multiphase regions with coarse W particles, scattered with C-rich or Ti-rich zones. The Ti-rich regions with an average %wt of 36.1% Ti) suggest the possible formation or segregation of TiC effects during powder mixing or treatment. Some Ti-enriched carbides or mixed W-Ti phases spots observed, might affect thermal and mechanical behaviour.

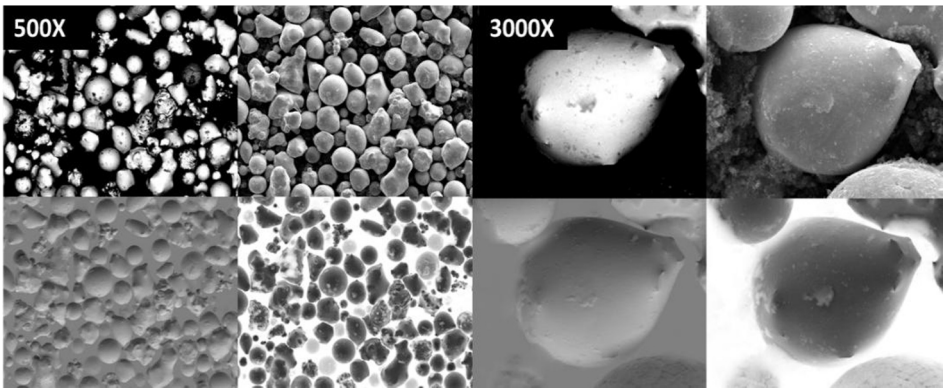

Fig. 13. SEM images of 15%Ti and 85% W at microscopic view at 500x and 3000x.

The powder sample of 15%Ti and 85% W exhibits a C dominance in full area scans of up to 88 wt%, with some zones having very low W ranging between 5–9 wt%. Localized EDS points depicted low Ti ranging from 1% to 7%, and a high presence of W, of up to 83%. A few areas were observed to have extremely W-rich (66–83% wt), implying particle clustering.

The 15% Ti and 85% W sample shows the most complex and heterogeneous structure amongst all the samples. The presence of high Ti and C concentrations suggest extensive TiC and WC formation or incomplete alloy mixing (contamination). The presence of W-rich phases implies incomplete diffusion or segregation, possibly affecting densification.

4 Conclusion

X-ray diffraction (XRD) analysis was successfully conducted on four powder samples comprising micron- and nano-sized Ti–W mixtures reacted with methane in a radio frequency plasma. The investigation revealed a systematic evolution of crystalline phases as a function of titanium content and particle size.

Key findings include:

- Microparticles depicted dominant phases of W_2C, W, and at higher Ti content resulting in the formation of $TiC_{0.47}H_{0.21}$, suggesting progressive formation of tungsten carbides and Ti-containing compounds as Ti content increased.
- Nanoparticles consistently depicted TiC and carbon (C) phases, especially those collected from the filter, indicating efficient conversion of Ti into titanium carbide during plasma processing.

- Reactor-collected nanoparticles at 15% Ti revealed more complex carbide formation, such as C_5Ti_8, suggesting different thermochemical conditions and potential secondary reactions in the reactor zone.
- A general trend observed was the diminishing presence of elemental tungsten (W) with increasing Ti content and processing time, implying that W was largely consumed in forming secondary carbide phases.
- The presence of broad peaks in nanoparticle XRD patterns indicates nanocrystallinity or poor crystallinity, in contrast to the sharper peaks seen in microparticle samples.

The particle size distribution of the various W-Ti powders compositions was strongly influenced by the titanium content. While low Ti content (1%) provided a narrow and predictable distribution ideal for precision applications, higher Ti levels (especially 15%) introduced variability that could benefit certain powder metallurgy applications but may pose challenges for uniform processing.

According to the SEM analysis results the following conclusion can be made:

- Ti content increases heterogeneity: From 1% to 15%, the compositions becomes increasingly irregular with more pronounced elemental segregation.
- Localized enrichment: At higher Ti%, the formation of TiC/W-Ti zones was more apparent and likely affects mechanical properties (e.g., increased hardness, brittleness).
- Microstructure–composition correlation: The PSD and EDS findings aligned broader particle size distributions correlate with compositional and phase heterogeneity.
- 1%–5% Ti powders are suitable for applications demanding uniform microstructures.
- 10%–15% Ti powders might be tailored for high-strength or wear-resistant applications, but may require post-processing (e.g., milling, sintering control).

References

1. K. Lu, J. Zhu, D. Guo, M. Yang, H. Sun, Z. Wang, X. Hui, and Y. Wu, Coatings 12, 1023 (2022).

https://doi.org/10.3390/coatings12071023

2. G Song., Y. Zhou., Y. Wang, J. Mater. Sci. **37**, 3541-3548 (2002).

http://dx.doi.org/10.1007/s11665-018-3287-9

3. H.C. Kim., D.K Kim., K.D Woo., I.Y Ko., I.J Shon, In. J. of Ref. Metals hard Mater **26**, 1, 48-54 (2008).

http://dx.doi.org/10.1007/s40820-019-0346-1

4. A. Roine, HSC Chemistry®, Outotec Research Oy

5. R.M. Dire, H. Bissett, D. Delport, and K. Premlall, *J. S. A. Inst. Min. Metall.* 121, 175–180 (2021).

6. V.P. Bondarenko and É.G. Pavlotskaya, *Powder Metall. Met. Ceram.* 34, 508–512 (1996).

https://dx.doi.org/10.1007/bf00559958

7. C.F. Davidson, G.B. Alexander, and M.E. Wadsworth, *Metall. Trans. B* **9**, 553–557 (1978).

https://doi.org/10.1007/BF03257203

8. R. Zhang, D. Liu, G.Q. Fan, H.B. Sun, J. Dang, and M. Lv, *Int. J. Energy Res.* 43, 4551 (2019).

https://doi.org/10.2298/JMMB231127011Z

9. J. Chappell and T. A. Ring, *Metall. Trans. B* 9, 553–557 (1986).

10. G. Miao, W. Du, Z.J. Pei, and C. Ma, *Additive Manufacturing* **58**, 103029 (2022).

http://dx.doi.org/10.1016/j.addma.2022.103029